Canadian Geotechnical Journal

Article

Analytical prediction of ground movements due to circular shaft construction in clayey soils

Chen Zheng[a], **Andrea Franza**[b], **and Rafael Jimenez**[a]

[a]ETSI Caminos, Canales y Puertos, Universidad Politécnica de Madrid, Madrid, Spain; [b]Department of Civil and Architectural Engineering, Aarhus University, Aarhus, Denmark

Corresponding author: **Andrea Franza** (anfr@cae.au.dk)

Abstract

With the rapid expansion of urbanization, shafts are needed to provide access to tunnelling projects or be utilized for permanent works. Their construction causes ground movements, affecting nearby foundations and buried infrastructure. This study presents an analytical equivalent volume loss approach for predicting three-dimensional ground movements resulting from a circular shaft construction: namely, ground losses in the elastic isotropic half space as a sequence of cavity contractions around the shaft are employed. First, the applicability and accuracy of proposed solutions are evaluated with published case studies and centrifuge tests. Thereafter, the method is employed to investigate the influence of the circular shaft construction on the surface and subsurface soil displacements. Considering design ground losses, this method allows for quick estimations of ground deformations and associated risk of serviceability losses.

Key words: shaft construction, ground movements, ground loss, analytical solution

Introduction

Vertical cylindrical excavations ('shafts') are commonly built in urban areas to provide access to tunnels or for ventilation. As for rectangular pits, soil deformations caused by the construction of a shaft will impact the nearby foundations of buildings, existing underground infrastructure, and services (among others; Son and Cording 2008; Ng et al. 2013). To avoid excessive displacements and deformations at existing structures, it is desirable to preliminary conduct a quick rational assessment of ground movements caused by circular shaft excavation.

Current studies on ground movements induced by deep excavations focused on rectangular pits (Yoo and Lee 2008; Ng et al. 2012, 2020; Teng et al. 2018; Hsiung 2020) for plane-strain excavations and rectangular pits; there have been successful applications of the elastic theory to vertical and horizontal displacement prediction (Ng and Yan 1998; Lei et al. 2001; Ng and Lei 2003; Fan et al. 2021). However, despite the availability of historical case studies of circular shaft construction (Wong and Kaiser 1988; Tan and Wang 2013; Faustin et al. 2017, 2018), which could be used to calibrate similar analytical solutions, practical methods for preliminary prediction of induced soil movements in shafts are limited to empirical methods (New and Bowers 1994; Le et al. 2019). In particular, New and Bowers (1994) presented an empirical formula to predict the surface settlements by shaft construction calibrated on the monitoring data from one shaft at Heathrow Express trial tunnel in stiff clay. The fitted coefficient of this empirical method is independent of the diameter and is applicable to circular shafts constructed in London Clay using similar construction methods (Schwamb and Soga 2015; Faustin et al. 2018). Recently, Faustin et al. (2018) reported field studies in London Clay and found that the ground movements around the shaft depend greatly on the construction technique, which can be classified into three categories: support before excavation (SBE) (e.g., diaphragm wall), excavation before support (EBS), and a combination of the two methods. Ground movements arising from the excavation of circular shafts using SBE are smaller compared with the EBS and combined method, which may also be characterized by a degree of overexcavation (as for tunnelling). In addition, the estimation of subsurface soil movements is also of interest; Le et al. (2019) performed centrifuge tests in kaolin clay to investigate the effects of pre-install shaft construction and suggested two empirical equations to describe the distributions of subsurface soil movements. Alternately, advanced numerical modelling (Schwamb and Soga 2015; Lai et al. 2020) is an effective tool for the design of shaft. However, a reliable analytical approach that can describe soil deformations during both shaft construction methods while overcoming the limitations of empirical methods has yet to be suggested and validated with physical measurements.

This paper aims to characterize displacements induced during circular shaft construction in clays. By employing spherical cavity contraction theory, the superposition method, and the concept of an equivalent volume loss, both vertical and horizontal ground movements around a circular

Fig. 1. (*a*) Equivalent volume-loss distribution induced by shaft excavation at depth *z*; (*b*) equal volume loss between cubic and spherical cavities; and (*c*) profile of the volume-loss strip losses along the shaft perimeter for $y = 0$.

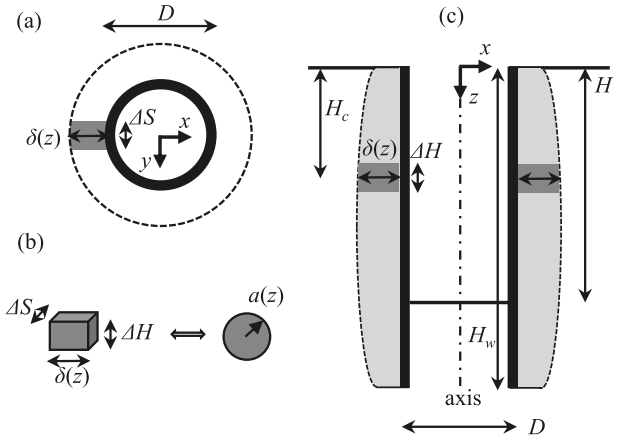

excavation are predicted. The applicability of the proposed methods is first evaluated against well-documented case histories and centrifuge tests in clays. Then, surface and subsurface movements by shaft construction are analyzed to understand ground deformation mechanisms induced by shafts.

Method

In this study, shaft-induced surface ground movements are indicated as $u_{z,0}$ and $u_{x,0}$, whereas subsurface displacements are denoted as u_z and u_x, respectively. To estimate the shaft-induced ground movements, the displacement field due to a distributed ground loss associated with the shaft construction can be computed by integrating ground losses occurring along the shaft's wall. Note that as a result of axisymmetric volume-loss distributions, the three-dimensional displacement field is described by radial displacement of soil pointing towards the axis centre, which in this study is quantified by horizontal u_x and vertical u_z in the plane *x*–*z* for $y = 0$ (see Fig. 1).

The analytical solution is based on the following assumptions: (i) the soil is assumed as an isotropic, homogeneous, and incompressible (undrained) medium; (ii) the wall deflection and overexcavation at the shaft are lumped into a three-dimensional volume loss V_l distributed around the shaft, obtained as solid of revolution by rotating around the central axis a vertical area with thickness $\delta(z)$ and distance $D/2$ from the central axis (see Figs. 1*a* and 1*c*); (iii) the three-dimensional volume loss distribution is discretized with each vertical strip regarded as a stack of spherical cavity losses along depth (see Figs. 1*a* and 1*b*); and (iv) the closed-form solutions of Pinto and Whittle (2014) for the three-dimensional displacement field caused by a spherical cavity contraction in the incompressible half space is considered. With respect to assumption (iii), the displacements in the three spatial directions (u_x^{cav}, u_y^{cav}, and u_z^{cav}) induced by a single spherical cavity with radius *a* and volume $V_l^{cav} = 4\pi a^3/3$ are

$$(1)\quad u_x^{cav} = \frac{V_l^{cav}}{4\pi}\left(\frac{x}{R_1^3} + (3-4\nu)\frac{x}{R_2^3} - \frac{6xz\,(z+H_c)}{R_2^5}\right)$$

$$(2)\quad u_y^{cav} = \frac{V_l^{cav}}{4\pi}\left(\frac{y}{R_1^3} + (3-4\nu)\frac{y}{R_2^3} - \frac{6yz\,(z+H_c)}{R_2^5}\right)$$

$$(3)\quad u_z^{cav} = -\frac{V_l^{cav}}{4\pi}\left(\frac{z-H_c}{R_1^3} - (3-4\nu)\frac{z+H_c}{R_2^3} + \frac{2z}{R_2^3} - \frac{6z(z+H_c)^2}{R_2^5}\right)$$

where *x*, *y*, and *z* are the horizontal and vertical spatial coordinates, H_c is the depth to the center of the cavity (see Fig. 1*b*), $\nu = 0.5$ is the Poisson's ratio for undrained conditions, $R_1 = \sqrt{x^2 + y^2 + (z - H_c)^2}$, and $R_2 = \sqrt{x^2 + y^2 + (z + H_c)^2}$. For the numerical integration, the perimeter of the shaft is divided into $n = H_w/\Delta H$ depth increments and $m = \pi D/\Delta S$ strips. Therefore, for the equal volume-loss approach (Chow and Teh 1990) shown in Fig. 1*b*, the equivalent radius of the spherical cavities *a* obtained by matching the volumes of the cubic cavity and of its equivalent spherical cavity is

$$(4)\quad a\,(z) = \sqrt[3]{\frac{3}{4\pi}\delta\,(z)\,\Delta S \Delta H}$$

The total three-dimensional displacement field of the soil (u_x, u_y, and u_z) is derived by superposition of the cavities of all strip volume losses as

$$(5)\quad u_x = \sum_{j=1}^{m}\sum_{i=1}^{n} u_{x,i,j}^{cav}, \quad u_y = \sum_{j=1}^{m}\sum_{i=1}^{n} u_{y,i,j}^{cav}, \quad u_z = \sum_{j=1}^{m}\sum_{i=1}^{n} u_{z,i,j}^{cav}$$

where *j* is the sequence number of strips and *i* is the sequence number of the depth increments. In this work, $\Delta S = 0.01$ m and $\Delta H = 0.01$ m are used.

Equivalent volume-loss distribution

The equivalent volume-loss distribution $\delta(z)$ may vary with depth, as shown in Fig. 1*c*, and it is a key input to the analytical prediction method. In real-world applications, $\delta(z)$ can be computed numerically, inferred from field or laboratory data, or set from the back-analysis of ground displacement data. For instance, it may be estimated as the horizontal displacement profile of the soil next to the constructed wall and the wall deflection for EBS and SBE shafts, respectively. Note that the monitoring of the soil displacement profile next to the shaft allows accounting for overexcavation in EBS compared with the use of the wall deflection measurements.

To characterize the input volume-loss distribution, the loss level β is defined as the ratio between the average thickness of the volume-loss strip $\bar{\delta}$ and H_w.

$$(6)\quad \beta = \bar{\delta}/H_w$$

$$(7)\quad \bar{\delta} = \frac{1}{H_w}\int_0^{H_w} \delta\,dz$$

It is of interest to illustrate the link between the dimensionless loss level β (or the average thickness of the volume loss $\bar{\delta}$)

and the shaft volume-loss parameter $V_{l,s}$ defined (similarly to tunnelling) as the ratio between the equivalent volume loss $V_l = \sum V_l^{cav} \approx \pi D \bar{\delta} H_w$ and the shaft volume $V_0 = \pi D^2 H_w/4$, as follows:

$$(8) \qquad V_{l,s} = \frac{V_l}{V_0} = \frac{4\bar{\delta}}{D} = \beta \frac{4H_w}{D}$$

In this paper, a parabolic shape for $\delta(z) = \beta(-6z^2/H_w + 6z)$ is chosen if not specified otherwise (as a first approximation); in these cases, the input parameters of the analytical method are limited to D, β, and H_w.

Validation

Ground movements used for validation were obtained from field monitoring by Faustin et al. (2017), New and Bowers (1994), and Newhouse (2017) in case histories using different construction methods in stiff clay in addition to the high-quality centrifuge test results of Le et al. (2019) conducted in clay. Table 1 summarizes final excavation depth (H), the wall length (H_w), the diameter of the shaft (D), the construction method, and the ground conditions.

Case 1: Heathrow Express trial tunnel (New and Bowers 1994)

The Heathrow Express shaft in stiff London Clay had an excavation depth of $H = 26$ m and a diameter $D = 11$ m, and it was constructed using the concurrent shaft sinking technique (precast segments of 16 m followed by a sprayed concrete lining (SCL) technique for the lower 10 m). The ground surface movements (settlements and radial surface movements) were monitored along T line; note that the radial displacement is equal to horizontal displacement along T line. Unfortunately, the original paper does not report the wall deflection or subsurface soil displacement data; thus, a parabolic volume loss $\delta(z)$ and relatively small loss levels (of $\beta = 0.05\%$–0.075%) were assumed to obtain similar level of settlements. Also, due to missing details, it was assumed $H_w = H$ for calculations.

Figure 2 compares monitoring and predicted surface movements against distance from the shaft's wall ($s = x - D/2$), with the monitoring data recorded when the shaft was approaching full depth of 26 m. Figure 2*a* shows that horizontal surface movements are well described by the analytical method for equivalent loss level of $\beta = 0.05\%$ and for points that are adjacent to the shaft (say, $s/H > 0.3$). However, the analytical predictions overestimate the horizontal movements at the 'close' region ($s/H < 0.3$). As shown in Fig. 2*b*, both the pattern and magnitude of ground settlements were well reasonably predicted using $\beta = 0.075\%$, and a spandrel-type settlement profile had developed after completion of the shaft.

Case 2: Crossrail TBM launch shaft at Limmo Peninsula (Faustin et al. 2017; Newhouse 2017)

Two shafts—referred to as 'main shaft' and 'auxiliary shaft'—were constructed at Crossrail's Limmo Peninsula tunnelling site to launch the TBMs and to provide the auxiliary TBM launch shaft, respectively. The 30 m diameter 'main shaft' excavation consists of the installation of a 53 m diaphragm wall (SBE) constructed before the excavation to be followed by a depth of 44 m of inner excavation; the 28 m diameter 'auxiliary shaft' consists of 14 m of steel sheet pile (SBE) and 25 m of SCL (EBS). The ground conditions at the shaft sites were typical of the London Basin strata (see Table 1). This case study provides a unique opportunity to examine the effect of different shaft construction methods on the magnitude of ground movements.

Figure 3*a* shows the input distribution δ of volume loss, while the predicted ground settlements are compared with the site monitoring data in Fig. 3*b*, where both ground settlements and horizontal offset from the shaft boundary are normalized by the excavation depth. To prepare this figure, the dewatering displacements were removed from the total settlements (Newhouse 2017). As it can be seen in Fig. 3*b*, the maximum surface settlement observed from the 'auxiliary shaft' excavation was about seven times larger than the maximum settlement observed from 'main shaft'. This may be due to the horizontal stress relief that relates to the retaining structure and overexcavation during the EBS method, which may cause greater settlements around the shaft than SBE. A very small volume-loss level ($\beta = 0.01\%$) would be required to reproduce the real wall deflection condition for a shaft constructed in stiff clay using the SBE method, whereas medium levels (of $\beta = 0.1\%$ and 0.15%) are reasonable for a shaft constructed in a similar geology using a combination of the EBS and SBE methods.

Centrifuge test in clay (Le et al. 2019)

A 1/100th centrifuge model was developed by Le et al. (2019) to investigate circular shaft excavation in overconsolidated Speswhite kaolin. The excavation was simulated in flight by draining heavy fluid from the annulus between the shaft liner and the soil. The prototype dimensions of the shaft corresponded to $D = 8$ m and $H_w = 20$ m. There are no wall deflection data reported from Le et al. (2019); thus, input δ is set equal to one-and-a-half times the horizontal movements measured by Le et al. (2019) at an offset of $5\% H_w$ (see Fig. 4*a*) to achieve an agreement between centrifuge and analytical horizontal movements at this distance.

Figures 4*b* and 4*c* compare the predicted and monitoring surface movements. Analytical settlements extend further away from the shaft ($s = H_w$) than measurements would suggest ($s = 0.6H_w$), as indicated by Fig. 4*b*. Similarly, Fig. 4*c* shows that the analytical result slightly overestimates the horizontal ground movements.

Next, subsurface movements are plotted in Fig. 5. The analytical horizontal soil displacements at the 'close' and 'mid-distance' sections ($s/H_w \leq 20\%$) match well the centrifuge data in Figs. 5*a*–5*c*, although the analytical predictions slightly overestimate the magnitude of soil horizontal displacement at the depth of the shaft toe. Also, the predicted settlements with depth in Figs. 5*e*–5*h* are in good agreement with the measurements, except for slight differences close to the wall (see subplot e). Despite this, the prediction of the level and shape of surface and subsurface movements is satisfactory. This statement is supported by the comparison of horizontal and vertical displacement contours from the

Table 1. Considered stratigraphies and corresponding pile bearing capacity.

No.	Shaft	Construction method	H_w (m)	H (m)	D (m)	Ground condition	Reference
1	Heathrow Express trial tunnel	Shaft sinking	–	26	11	Superfical deposits (3.5 m) London Clay	New and Bowers (1994)
2	Limmo Peninsula main shaft	Diaphragm wall	53	44	30	Superficial deposits (17 m) London Clay (31 m) Lambeth Group (18 m)	Faustin et al. (2017) Newhouse (2017)
3	Limmo Peninsula auxiliary shaft	Sheet piles SCL	39	39	28	Superficial deposits (16.7 m) London Clay (75 m) Lambeth Group (6.3 m)	Faustin et al. (2017) Newhouse (2017)
4*	Centrifuge test	Pre-installed shaft lining	20	20	8	Speswhite kaolin	Le et al. (2019)

Note: SCL, sprayed concrete lining.

Fig. 2. Monitoring data from New and Bowers (1994) and its comparison with analytical predictions.

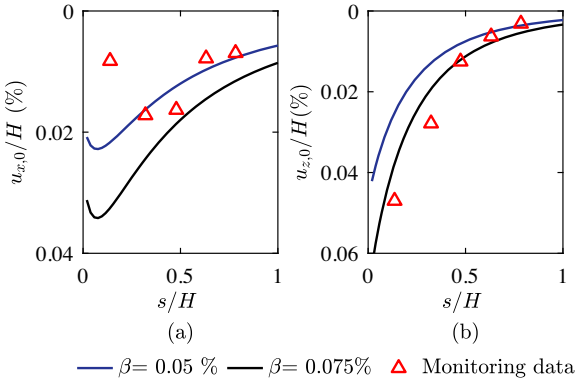

Fig. 3. Observed and predicted settlement during excavation of Crossrail's main and auxiliary shafts at Limmo Peninsula (Newhouse 2017).

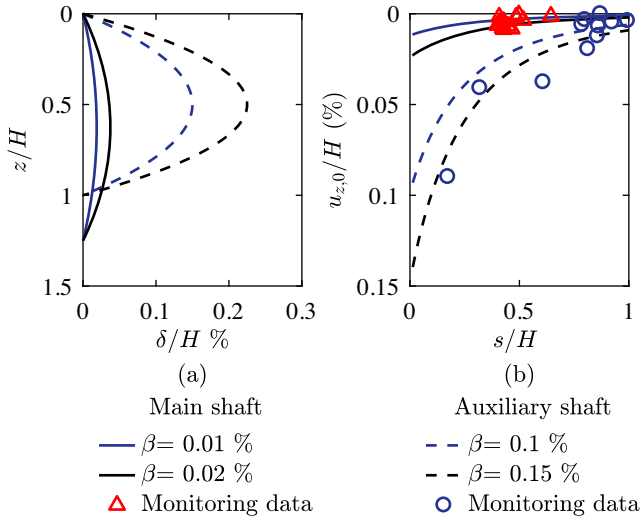

centrifuge data and from the analytical results in Fig. 6, confirming similar deformation patterns for analytical and centrifuge modelling in soil conditions similar to those tested by Le et al. (2019).

Parametric results

A parametric study is carried out considering shaft diameters $D = 10$, 20, and 30 m for a wall depth of $H_w = 30$ m, assuming a parabolic volume-loss profile (Wong and Kaiser 1988; Tan and Wang 2013). Results are presented in normalized form.

Figures 7*a* and 7*b* show the shape of the surface profiles as the relationship between the normalized ground surface movements ($u_{z,0}/u_{z,0}^{max}$ and $u_{x,0}/u_{x,0}^{max}$) and the normalized distance from the wall (s/H_w). The variation of shaft diameter has marginal effects on the shape of surface settlements and horizontal movements. Interestingly, spandrel-type settlements occur in all cases, consistently with the empirical formula of New and Bowers (1994), whereas horizontal movement profiles have 'tick type'. The influence zone of horizontal movements is wider, with analytical horizontal movements extending to more than 1 times the wall length, hence being wider than the surface settlement trough. Figures 7*c* and 7*d* plot the maximum ground surface movements against the maximum lateral displacement of the volume loss. Both of these are normalized by wall depth. Movements increase linearly with δ^{max}, as expected. Also, analytical maximum surface movements increased with the shaft diameter, particularly between $D = 10$ m and 20 m. The ratio between maximum surface settlement and maximum volume loss displacement (or wall deflection) $u_{z,0}^{max}/\delta^{max}$ is within the range of 0.55 to ≈0.6, which slightly underestimates the field data from Tan and Wang (2013) and Wong and Kaiser (1988). These magnitudes of the ground settlement are slightly smaller than the results reported by Moormann (2004) for deep excavation in soft clay ($u_{z,0}^{max}/\delta^{max} = 0.5 - 2.0$). On the other hand, normalized maximum horizontal surface movements of $u_{x,0}^{max}/\delta^{max} = 0.28 - 0.36$ are given by the solution. Therefore, maximum surface horizontal displacement is approximately half the value of the maximum surface settlement ($u_{x,0}^{max}/u_{z,0}^{max} \approx 0.5 - 0.6$), which is similar compared with the observed data in case studies (New and Bowers 1994).

Next, subsurface movements are discussed. Figure 8*a* shows the subsurface settlement profiles at various depths ($z/H_w = 0 - 0.6$). The normalized settlement $u_z/H_w \times \beta$ is plotted against s/H_w. With the increase of depth, the settlement profile gradually changes from spandrel to concave

Fig. 4. Volume loss input and surface soil displacements in centrifuge test (Le et al. 2019).

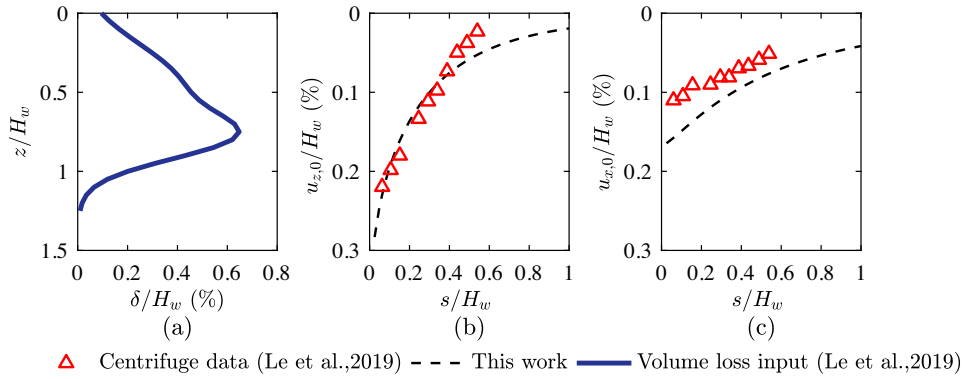

Fig. 5. Subsurface soil displacements in centrifuge test (Le et al. 2019).

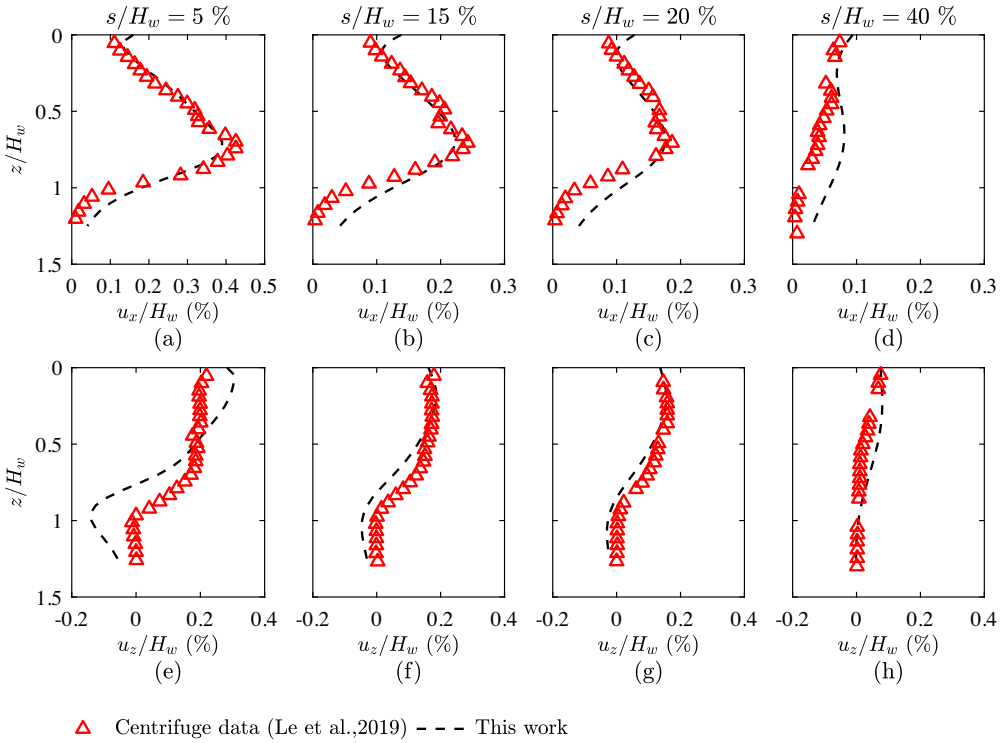

shape, and the magnitude of settlements decreased gradually. Figure 8*b* shows the subsurface horizontal movements at various depth. Results indicate that the shape of the horizontal movement profiles evolve into a spandrel shape distribution as depth increases. The magnitude of horizontal movements increases with depth at sections close to wall ($s/H_w < 0.3$), which is opposite to the evolution of subsurface settlements. Figure 9 presents subsurface vertical and horizontal movements at various distances ($s = 0.1$–$0.6\ H_w$) from the shaft wall. Results close to the wall ($s = 0.1H_w$) indicate a sharp decrease of subsurface settlements with depth, which could even lead to upwards soil movements near the wall toe; however, settlements at the sections $s = 0.4H_w$ and $0.6H_w$ are much smaller than those obtained 'close' to the wall, with settlements that linearly decrease (slightly) with depth, as shown in Fig. 9*a*. Figure 9*b* indicates that subsurface horizontal movements follow the parabolic wall deflection shape at sections $s = 0.1H_w$ and $0.2H_w$ and that the horizontal movement profiles attenuate their magnitude with increasing distance from the wall.

Design guidance to estimate

Figures 10*a* and 10*b* display contour lines of the normalized horizontal and vertical displacements for a typical shaft (diameter $D = 20$ m, wall depth of $H_w = 30$ m, and average displacement of $\bar{\delta} = 30$ mm or $\beta = 0.1\%$; parabolic wall deflection shape), as predicted by the analytical model. These are compared with analytical results in Figs. 10*c* and 10*d* obtained for a long deep excavation (i.e., under plane-strain condition) carried out using identical excavation parameters and a similar analytical prediction method proposed (Zhang et al. 2011).

Fig. 6. Comparison with the centrifuge test displacement contours from Le et al. (2019) (at model scale).

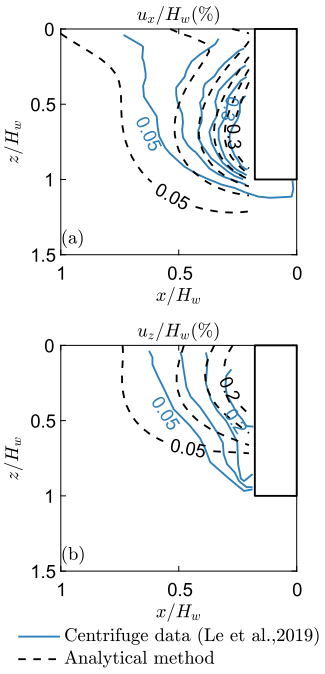

Fig. 7. Shapes of surface (*a*) settlements and (*b*) horizontal movements. Normalized maximum surface (*c*) settlement and (*d*) horizontal displacement against maximum lateral displacement of the wall, the former compared with field data.

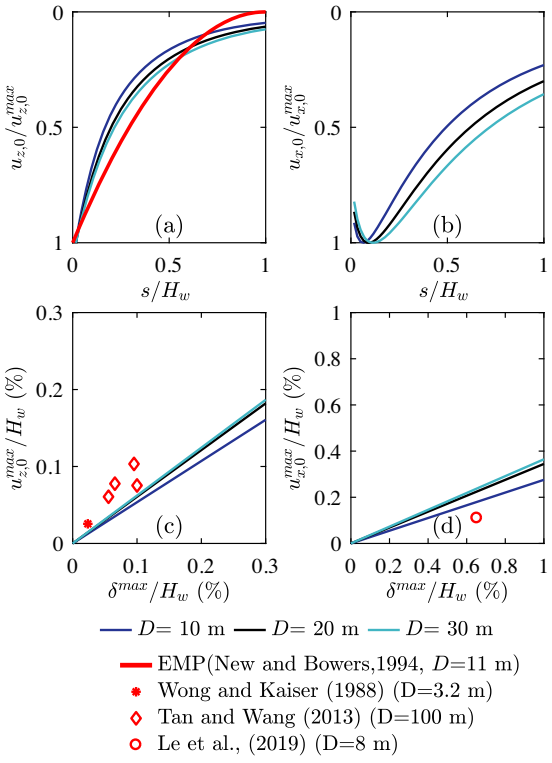

As expected, the magnitude of radial ground movements induced by the shaft is relatively smaller than that of transverse movements associated with the long deep excavation.

Fig. 8. Subsurface soil movement profiles at various depths from the surface.

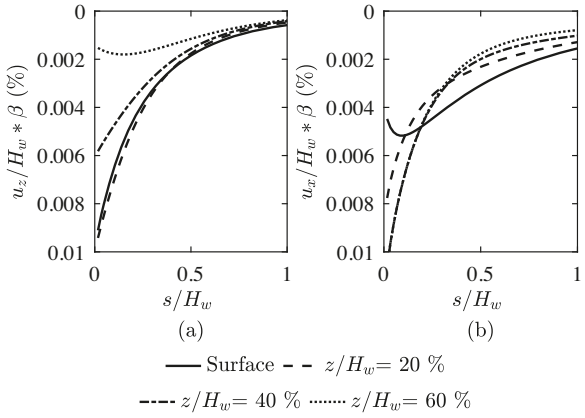

Fig. 9. Subsurface soil movement profiles at various distances from the shaft.

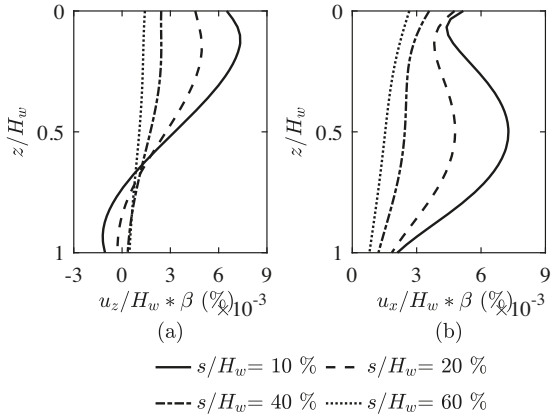

However, the shape of the subsurface deformation pattern is rather similar for the two excavation types.

Conclusion

This paper presents an analytical method, combining cavity contraction theory in an incompressible half space and equivalent volume-loss approach, to predict surface and subsurface vertical and horizontal ground movements induced by shaft construction in clayey soil. Inputs of this analytical solution are the magnitude and the distribution shape of the equivalent volume loss at the shaft wall.

The analytical predictions of the analytical method compared well with monitoring field data of shaft construction. From this comparison, it is concluded that, when using the analytical modelling, the ratio β between the average thickness of the equivalent volume loss and the wall height is expected to be very small for the SBE construction method in stiff clay ($\beta = 0.01\%$–0.02%), whereas it can be slightly higher for the EBS and combined methods ($\beta = 0.05\%$–0.1%). The ground movement level is controlled by the shaft's volume loss level β and shaft depth (the latter observation in agreement with empirical methods in the literature), whereas the

Fig. 10. Displacement contours caused by (*a*) shaft construction and (*b*) plane-strain deep excavation: (left) settlements and (right) horizontal movements for $\beta = 0.1\%$.

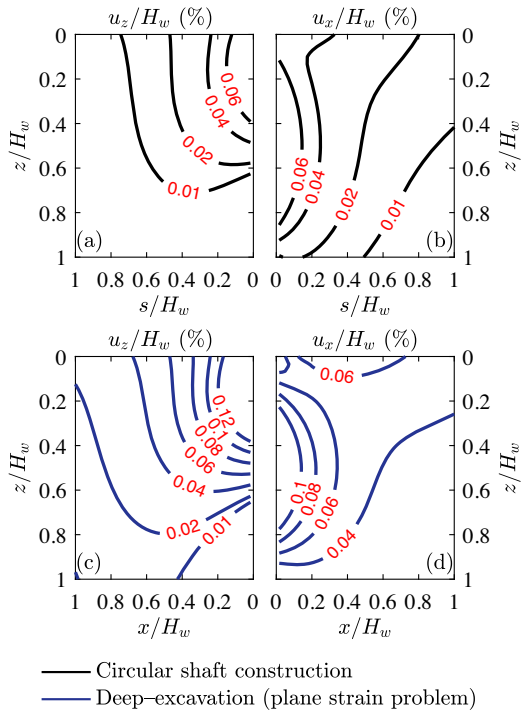

effect of the shaft diameter is limited for typical values up to 30 m. This confirmed the importance of considering the construction method.

The analytical solution predicts spandrel-shaped settlement profiles both at the surface and subsurface for circular shaft construction when the equivalent volume loss has a parabolic shape with depth. The maximum surface settlement ranges between 0.55 and 0.6 times the maximum amplitude of parabolic volume losses, with the latter being similar to the maximum wall deflection for SBE shafts. The horizontal surface movement distribution had tick profiles, with maximum horizontal surface movements being approximately half the maximum settlement. The subsurface soil deformation pattern predicted with the proposed method agreed with centrifuge measurements, confirming that subsurface settlements reduce along the shaft's depth, whereas horizontal movement variation with depth is modest along the shaft. Construction methods employing circular shafts are hence expected to induce smaller ground movements than construction methods employing deep excavations as rectangle pits, even though both may have similar subsurface deformation patterns.

The proposed method can be used to assess how controlling the wall deflection and overexcavation can reduce ground movements in practical engineering. In combination with equivalent volume losses obtained from previous case studies, this analytical method can facilitate the prediction of soil displacements and of resulting interaction deformations of nearby structures, which can be useful for a quick evaluation of the need for mitigation measures. However, as previously discussed (Sagaseta 1987; Alonso 2018), engineering judgement is needed when applying simple elastic theories to excavation- and volume loss-induced problems.

List of symbols

a	radius of the spherical cavity
D	diameter of shaft
s	distance from the wall
H_c	cavity depth
H	excavation depth
H_w	wall length
u_x	horizontal subsurface movements
u_x^{cav}	horizontal movements due to a cavity volume loss
$u_{x,0}$	horizontal surface movements
$u_{x,0}^{max}$	maximum horizontal surface movements
u_z	vertical subsurface movements
u_z^{cav}	vertical movements due to a cavity volume loss
$u_{z,0}$	vertical surface movements
$u_{z,0}^{max}$	maximum vertical surface movements
V_s	shaft volume loss
V_l	equivalent volume loss
x	horizontal spatial coordinate (x-axis)
y	horizontal spatial coordinate (y-axis)
z	vertical spatial coordinate
β	ratio between average thickness of the volume-loss strip and wall height
ΔH	length of the wall segment
ΔS	width of the strip
δ	thickness of the volume loss strip
$\bar{\delta}$	average thickness of the volume loss strip
ν	Poisson's ratio of soil

Acknowledgements

This project has received funding from the European Union's Horizon 2020 research and innovation programme under the Marie Sklodowska–Curie grant agreement no. 793715. Partial support was also provided by the Spanish Ministry of Science and Innovation, under Grant PID2019-108060RB-I00. The first author also received financial support provided by the China Scholarship Council (CSC) scholarship no. 201706930026.

Article information

History dates

Received: 29 July 2022
Accepted: 6 October 2022
Accepted manuscript online: 24 January 2023
Version of record online: 22 June 2023

Copyright

Author information

Author ORCIDs

Chen Zheng https://orcid.org/0000-0002-9028-3811
Andrea Franza https://orcid.org/0000-0002-8510-0355

Author contributions

Conceptualization: AF, RJ
Formal analysis: CZ
Funding acquisition: RJ
Methodology: CZ, AF
Software: CZ, AF
Supervision: AF, RJ
Validation: CZ
Writing – original draft: CZ
Writing – review & editing: AF, RJ

References

Alonso, E.E. 2018. Tunnelling in urban environments: protecting sensitive buildings. *In* Proceedings of the China–Europe Conference on Geotechnical Engineering. pp. 1117–1127. doi:10.1007/978-3-319-97115-5_51.

Chow, Y.K., and Teh, C.I. 1990. A theoretical study of pile heave. Géotechnique, **40**(1): 1–14. doi:10.1680/geot.1990.40.1.1.

Fan, X.Z., Phoon, K.K., Xu, C.J., and Tang, C. 2021. Closed-form solution for excavation-induced ground settlement profile in clay. Computers and Geotechnics, **137**: 104266. doi:10.1016/j.compgeo.2021.104266.

Faustin, N.E., Elshafie, M.Z.E.B., and Mair, R.J. 2018. Case studies of circular shaft construction in London. Proceedings of the Institution of Civil Engineers—Geotechnical Engineering, **171**(5): 391–404. doi:10.1680/jgeen.17.00166.

Faustin, N.E., Mair, R.J., Elshafie, M.Z.E.B., Menkiti, C., and Black, M. 2017. Field measurements of ground movements associated with circular shaft construction. *In* Geotechnical aspects of underground construction in soft ground. CRC Press. pp. 301–308. doi:10.1201/9781315099507-35.

Hsiung, B.C.B. 2020. Observations of the ground and structural behaviours induced by a deep excavation in loose sands. Acta Geotechnica, **15**(6): 1577–1593. doi:10.1007/s11440-019-00864-0.

Lai, F., Liu, S., Deng, Y., Sun, Y., Wu, K., and Liu, H. 2020. Numerical investigations of the installation process of giant deep-buried circular open caissons in undrained clay. Computers and Geotechnics, **118**: 103322. doi:10.1016/j.compgeo.2019.103322.

Le, B.T., Goodey, R.J., and Divall, S. 2019. Subsurface ground movements due to circular shaft construction. Soils and Foundations, **59**(5): 1160–1171. doi:10.1016/j.sandf.2019.03.013.

Lei, G.H., Ng, C.W.W., and Rigby, D.B. 2001. Stress and displacement around an elastic artificial rectangular hole. Journal of Engineering Mechanics, **127**(9): 880–890. doi:10.1061/(ASCE)0733-9399(2001)127:9(880).

Moormann, C. 2004. Analysis of wall and ground movements due to deep excavations in soft soil based on a new worldwide database. Soils and Foundations, **44**(1): 87–98. doi:10.3208/sandf.44.87.

New, B.M., and Bowers, K.H. 1994. Ground movement model validation at the Heathrow Express trial tunnel. *In* Tunnelling '94. pp. 301–329. doi:10.1007/978-1-4615-2646-9_19.

Newhouse, J. 2017. Ground movement due to shaft construction. Master's thesis, Imperial College London, London, England.

Ng, C.W.W., and Lei, G.H. 2003. An explicit analytical solution for calculating horizontal stress changes and displacements around an excavated diaphragm wall panel. Canadian Geotechnical Journal, **40**(4): 780–792. doi:10.1139/t03-027.

Ng, C.W.W., and Yan, R.W.M. 1998. Stress transfer and deformation mechanisms around a diaphragm wall panel. Journal of Geotechnical and Geoenvironmental Engineering, **124**(7): 638–648. doi:10.1061/(ASCE)1090-0241(1998)124:7(638).

Ng, C.W.W., Hong, Y., Liu, G.B., and Liu, T. 2012. Ground deformations and soil–structure interaction of a multi-propped excavation in Shanghai soft clays. Géotechnique, **62**(10): 907–921. doi:10.1680/geot.10.P.072.

Ng, C.W.W., Shi, J., and Hong, Y. 2013. Three-dimensional centrifuge modelling of basement excavation effects on an existing tunnel in dry sand. Canadian Geotechnical Journal, **50**(8): 874–888. doi:10.1139/cgj-2012-0423.

Ng, C.W.W., Zheng, G., Ni, J., and Zhou, C. 2020. Use of unsaturated small-strain soil stiffness to the design of wall deflection and ground movement adjacent to deep excavation. Computers and Geotechnics, **119**: 103375. doi:10.1016/j.compgeo.2019.103375.

Pinto, F., and Whittle, A.J. 2014. Ground movements due to shallow tunnels in soft ground. I: analytical solutions. Journal of Geotechnical and Geoenvironmental Engineering, **140**(4): 04013040. doi:10.1061/(ASCE)GT.1943-5606.0000948.

Sagaseta, C. 1987. Analysis of undrained soil deformation due to ground loss. Géotechnique, **37**(3): 301–320. doi:10.1680/geot.1987.37.3.301.

Schwamb, T., and Soga, K. 2015. Numerical modelling of a deep circular excavation at Abbey Mills in London. Géotechnique, **65**(7): 604–619. doi:10.1680/geot.14.P.251.

Son, M., and Cording, E.J. 2008. Numerical model tests of building response to excavation-induced ground movements. Canadian Geotechnical Journal, **45**(11): 1611–1621. doi:10.1139/T08-074.

Tan, Y., and Wang, D. 2013. Characteristics of a large-scale deep foundation pit excavated by the central-island technique in Shanghai soft clay. I: bottom-up construction of the central cylindrical shaft. Journal of Geotechnical and Geoenvironmental Engineering, **139**(11): 1875–1893. doi:10.1061/(ASCE)GT.1943-5606.0000928.

Teng, F., Arboleda-Monsalve, L.G., and Finno, R.J. 2018. Numerical simulation of recent stress-history effects on excavation responses in soft clays. Journal of Geotechnical and Geoenvironmental Engineering, **144**(8): 06018005. doi:10.1061/(ASCE)GT.1943-5606.0001921.

Wong, R.C.K., and Kaiser, P.K. 1988. Behaviour of vertical shafts: reevaluation of model test results and evaluation of field measurements. Canadian Geotechnical Journal, **25**(2): 338–352. doi:10.1139/t88-035.

Yoo, C., and Lee, D. 2008. Deep excavation-induced ground surface movement characteristics—a numerical investigation. Computers and Geotechnics, **35**(2): 231–252. doi:10.1016/j.compgeo.2007.05.002.

Zhang, R., Zheng, J., Pu, H., and Zhang, L. 2011. Analysis of excavation-induced responses of loaded pile foundations considering unloading effect. Tunnelling and Underground Space Technology, **26**(2): 320–335. doi:10.1016/j.tust.2010.11.003.